Journal of Applied Fluid Mechanics, Vol. 12, No. 3, pp. 751-762, 2019.
Available online at www.jafmonline.net, ISSN 1735-3645, EISSN 1735-3645.
DOI: 10.29252/jafm.12.03.29242

Influence of the Presence of the Lorentz Force and its Direction on the Suppression of Secondary Flow in Two Different Orifices: A Numerical Study using OpenFOAM

R. J. Singh and T. B. Gohil†

Department of Mechanical Engineering, Visvesvaraya National Institute of Technology, Nagpur, India - 440010

†*Corresponding Author Email: trushar.gohil@gmail.com*

(Received June 1, 2018; accepted September 17, 2018)

ABSTRACT

The present analysis emphasized the presence of Lorentz force and its directional effect on the fluid flow and its structure in the channel with two differently shaped orifices. The flow through orifice causes the generation of the bubbles or eddies in the downstream flow. In this study, the numerical code is developed in the open source CFD tool kit OpenFOAM. The magnetohydrodynamics (MHD) principle is adopted to achieve the present objectives. Direct numerical simulation (DNS) has been carried out to predict the flow features at fixed Reynolds number of Re = 1000 and blockage ratio of 1:4 with the varying magnetic field. The magnetic field is varied in term of Hartmann number (Ha) in the direction normal to the flow of fluid. The induced Lorentz force considerably occupies the wake flow area downstream of the throat and hence suppressed down the vortices in the flow. The results obtained has the promising effect of suppressing down the vortex flow past two different orifices produced by the electromagnetic pressure gradient. The present study shows the MHD based flow can be significantly employed for the flow past orifice or any arbitrary obstacle in order to achieve the flow without wake region. The current analysis suggests the method of vortex control by producing Lorentz force using magnetic field without modification of geometry or additional use of devices into the system.

Keywords: OpenFOAM; Magnetohydrodynamics; DNS; Vortex control; Pressure drop.

NOMENCLATURE

B	magnetic field	U	average velocity
d	orifice width	x, y	cartesian co-ordinates
D	channel width		
Ha	hartmann number	β	blockage ratio
j	current density	μ	dynamic viscosity
L	channel length	ν	kinematic viscosity
p	pressure	ϕ	electric potential
Re	reynolds number	ρ	density of fluid
t	orifice thickness	σ	electric conductivity

1. INTRODUCTION

The most common device used for the measuring flow of fluid is orifice meter. However, the flow past orifice has certain flow related issues likes cavitation, flow assisted corrosion and erosion of the pipe due to bubbles formation. The sudden expansion or contraction in the path of the flow of fluid leads to the generation of pressure drop, Reynolds stresses, and large vortex structures. The other application of orifice is as flow limitation device with pressure control. Although, the implementation of restriction orifice has various flow related complications like cavitation, erosion of the pipeline in the presence of solid obstacles, noise, and vibrations. The restricting orifice may have multiple holes for achieving the lower pressure (Haimin *et al.*, 2013). The wake region downstream of the orifice has various scaling vortex causes the cavitation or impingement of particles on the surface of the pipe. It is the main source of the pipe wall erosion of pipeline in nuclear or fossil power

plant. The cavitation in the pipe leads to the formation of bubbles, which causes the mechanical wear on the surface. The flow assisted corrosion (FAC) is electrochemical corrosion process. Where the preventive oxide coating on the metallic surfaces dissolves into the chaotic stream of fluid. Thus, the metal thickness of the pipe degraded and reaches below the critical thickness necessary to tolerate operational stresses. FAC has influenced by several parameters, like flow velocity, dissolved oxygen content, material constituents, temperature, etc., and it is the highly fatal corrosion process for the pipe made up of carbon steel material (Kain, 2014; Utanohara *et al.*, 2012).

The chaotic flow past orifice or backward stepping face has the significant role in the bubbles formation and erosion of the metallic channel. Therefore, several kind of research have been performed in the area of the flow past contraction and expansion or orifice in the channel to reduce the wake zone. The numerical solution is the preferable way to obtain the complete solution with the understanding of different flow regions, like reattachment zone, primary recirculation region, secondary recirculation in the corner vortex, etc. Singh and John (2015) had performed the numerical analysis using ANSYS CFX to determine the effect of flow and geometrical parameters on discharge coefficient and concluded that the reattachment point in the multiple orifices is nearer than the single orifice. Hollingshead *et al*. (2011) investigated the relation between Reynolds number and coefficient of discharge for the different shape of flow meters using ANSYS FLUENT.

It has been indicated that for low Re, the decrease in the Re causes the rapid decrease in the coefficient of discharge for venturi, V-cone, and wedge flow meters. For orifice meter, the coefficients of discharge initially increase with the decrease in the *Re* to the maximum and then sharply decreased with the further decrease in *Re*. Shah *et al*. (2012) performed the numerical simulation using the OpenFOAM and correlate with the experimental data of Morrison *et al*. (1993) to propose the location of pressure tap at vena-contracta to quantify the flow with improved accuracy and sensitivity. Abdulrazaq *et al*. (2017) had numerically studied the pressure control in the pipe with multiple restricting orifices to achieve either higher or lesser pressure drop. The least and higher pressure drop is achieved in the case of double orifice alignment with one and two pipe diameter spacing respectively. Another type of active forcing like electrohydrodynamic (EHD) or magnetohydrodynamics (MHD) are used to control the flow separation and the formation of primary and secondary vortices. Deylami *et al*. (2017) and Sreenivasan *et al.* (2000) carried out the numerical analysis to suppress the flow past circular cylinder using EHD actuator. It has been concluded that the increase in the applied voltage decrease the vortices behind the cylinder and the drag coefficient changes with the modification in the shape of the grounded electrode. Mardkari *et al*. (2012) experimentally determined the influence of EHD actuator on the fluid flow past bluff body of cylindrical cross-section and showed total drag suppression. Yakeno, *et al*. (2015) established two-dimensional excitation induced by plasma actuator with dielectric barrier discharge to control the separation and reattachment of flow over the hump. The reattachment is imposed by excitation control with increasing the turbulence fluctuation. Shan *et al*. (2016) experimentally reveals the influence of the orifice to pipe diameter ratio (β) on the flow past the square-edged orifice. PIV system is used to measure the velocity fields and reattachments zone. Authors reported that the local Reynolds stress is independent of blockage ratio (β) in the shear-layer zone close to the orifice. El Khoury *et al*. (2010) had performed DNS of turbulent flow through the orifice with the blockage ratio of 1:2, and concluded that the flow profile is asymmetric due to Coanda effect and long streamwise domain past orifice is needed for periodic boundary conditions to get the symmetric profile.

Literature shows various methods to control the flow separation and formation of vortices. It can be categorized in the three section such as: Active, Passive and compound. The active flow control methods are EHD, MHD, surface vibration and acoustic fields. The passive controls are accomplished by redesigning the geometry or by adding the dimples or tapes on the surface. The compound technique is just the combination of both active and passive methods. The active controls methods other than MHD needs the power consumption for the operation. Therefore, MHD has been the widely used in the area of the flow pattern control method. With the application of magnetic field the flow separation is controlled due to the development of Lorentz force and fluids are forced to flow in a uniform layer and near to the wall. The magnetic field stabilized and suppressed the asymmetry pattern of fluid with the formation of equally sized recirculation zone in the back step channel (Mistrangelo *et al.*, 2007; *Vantieghem et al.*, (2009)). Altintas and Ozkol (2015) had performed the MHD based flow in the circular pipe where it has been observed that the flow in the pipe gets slows down with an increase in the magnetic field.

According to the above literature, it is observed that the most of the researchers have discussed about the control of wake flow past orifice and pressure drop in the channel by incorporating different methods like, redesigning the geometry, EHD, surface vibration, acoustic field and MHD. However, in the case of MHD, limited attention is observed towards the study of the effect of the generation of Lorentz force and its strength with different orientation in the channel on the vortex flow. It is the sole responsible for wake control and rise in the pressure drop in the downstream of the flow. The main objective of the present analysis is to study the effect of the presence of Lorentz force with its strength and directional effect in the downstream of orifice flow. The simulation is performed using in-house developed the MHD based flow solver on the OpenFOAM platform using electric potential formulation.

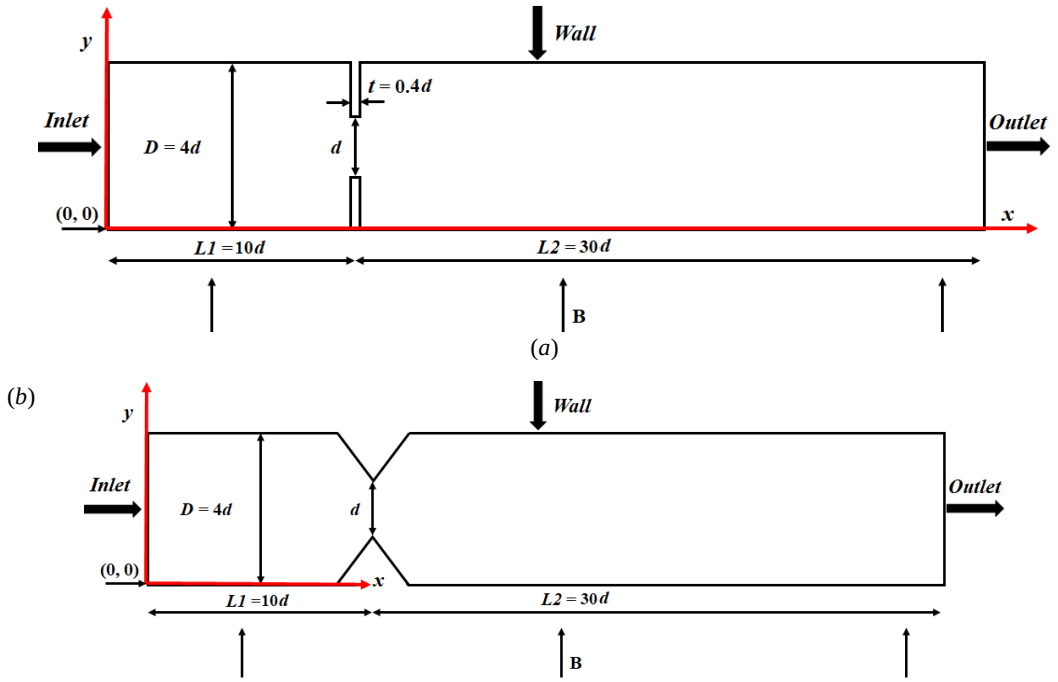

Fig. 1. Schematic drawing and geometrical detail of channel with (*orifice -1*) rectangular plate orifice (a), and (*orifice -2*) triangular shaped orifice (b).

2. PROBLEM DEFINITION

To characterize the effect of applied magnetic field, two type of orifice are considered within the channel flow. The considered two-dimensional orifices are rectangular plate orifice (*Orifice 1*) and triangularly shaped orifice (*Orifice 2*) as shown in Figs. 1 (a and b). The wall of the channel is electrically insulated. Here, *D* is the width of the channel and *d* is the entry width of the orifice. *L1* and *L2* are the upstream and downstream channel length respectively. The entry width *d* of orifice and channel width *D* has the value of 0.5 and 2 respectively. The blockage ratio is defined as "$\beta = d/D$" has a value of 1:4. The numerical solution for the present study is carried out at four different Hartmann number (*Ha* = 0, 50, 100, and 200) for flow through both the orifices. The Reynolds number is fixed for both cases as *Re* = 1000, and it is defined by the entry width of the channel.

3. MATHEMATICAL EQUATIONS

The flow field features of incompressible and laminar flow through both the orifices in the channel is obtained by solving continuity and momentum equations. The Navier-Stokes equation is only capable of determining the hydrodynamic behavior of fluid flowing through the channel. To capture the flow behavior in MHD and to enable the magnetic suppressing effect in the fluid, the Lorentz force ($j \times B$) term is included in the momentum equation as a source term. The complete set of the equations is described as follow.

Continuity equation

$$\nabla \cdot \vec{U} = 0 \tag{1}$$

Momentum transfer equation

$$\frac{\partial \vec{U}}{\partial t} + (\vec{U} \cdot \nabla)\vec{U} = -\frac{\nabla p}{\rho} + \nu \cdot \nabla^2 \vec{U} + \frac{\vec{j} \times \vec{B}}{\rho} \tag{2}$$

Ohm's law of current density

$$\vec{j} = \sigma(-\nabla \phi + \vec{U} \times \vec{B}) \tag{3}$$

Conservation of charge

$$\nabla \cdot \vec{j} = 0 \tag{4}$$

Poisson's equation of electric potential

$$\nabla^2 \phi = \nabla \cdot (\vec{U} \times \vec{B}) \tag{5}$$

Lorentz force

$$F_L = \vec{j} \times \vec{B} \tag{6}$$

The electric potential (Eq. 5) is obtained by comparing the Ohm's law of current density (Eq. 3) and conservation of charge (Eq. 4). In the above set of the equations, the variables *U*, *p*, *B*, *j*, and ϕ represents the average inlet velocity, pressure, magnetic field, current density and electric potential respectively. Whereas, the ρ, μ, ν and σ are the fluid properties stands for density, dynamic viscosity, kinematic viscosity and electric conductivity of fluid respectively. The two non-dimensional control parameters are used in this case that governs the fluid flow under the influence of magnetic field are Hartman number ($Ha = BD\sqrt{\sigma/\mu}$) and Reynolds

number ($Re = \rho UD/\mu$). Here, *Ha* defines the ratio of electromagnetic force to the viscous force. The physical properties of the fluid are assumed to be constant throughout the analysis.

4. SOLVING ALGORITHM, METHODOLOGY AND GRID INDEPENDENCE TEST

The Direct Numerical Simulation (DNS) is performed on the open source CFD tool kit OpenFOAM. The above set of governing equations (Eq. (1 – 6)) is solved by using finite volume discretization method. The flow of solution for the present solver is based on PIMPLE algorithms as follows.

a) Initialize all the variable fields.

b) The PIMPLE loop is used to solve Eqs. (1) and (2). The Rhie and Chow (Ferziger and Peric, 2002) interpolation scheme is functioning to obtain pressure and velocity. Here, the velocity is calculated by solving momentum equation and pressure is calculated by pressure Poisson equation derived from continuity equation.

c) The Eq. (5) is then solved to obtain the electric potential. After that, the electric potential value is replaced in the current density Eq. (3) to get updated electric current density.

d) The Lorentz force is getting calculated by the taking cross product of generated electric current density with the imposed magnetic field as per the Eq. (6) at each cell.

e) Update the velocity, pressure and Lorentz force term in the momentum Eq. (2).

f) Go to the next iteration.

The first order accurate Euler scheme is used to solve the temporal terms, and second-order central difference scheme is used for the convective and diffusive terms. The under-relaxation factors for velocity and pressure as 0.7 and 0.3 respectively are set to stabilize the flow. The adjustable rum time mode with Courant number (C_o) equal to one is considered. The PIMPLE loop with two outer correctors is employed in the solution to achieve the faster convergence for velocity and pressure. The tolerance level for all the field variables *B, U, p, T,* and ϕ is set as 10^{-6}. The boundary conditions and non-dimensional parameters used for both geometries are mentioned in the following Table 1.

The grid independence test is performed to identify the sufficiently resolved grid size so that the solution does not change by the further increase in the grid elements. The grid independence computation is carried out at fixed Reynolds number of 1000 and *Ha* of 100 in both cases. The considered three grid size for both orifice are "grid 1 = 60,000, grid 2 = 100,000 and grid 3 = 140,000". Figures 2 (a, b) shows the variation of streamwise velocity along the axial direction obtained for three different grids. It is observed from the Figs. 2 (a, b) that the all the grid size used for the present case is fine enough to get the uniform pattern. Hence, grid 2 (100,000) is chosen for further computation in both cases. To perform DNS, the fine mesh is required near the wall to capture the near wall phenomena. In the considered grid size, the minimum space between the grids near the wall is maintained as 10^{-4} with 6-8 elements in the Hartmann layers to capture the flow behavior in the boundary layers, and the maximum grid size in the core volume is 0.015.

Table 1 Boundary conditions and non-dimensional parameters

Parameters	Inlet	Outlet	Walls
U	1	$\partial U/\partial n = 0$	No slip
p	$\partial p/\partial n = 0$	$p = 0$	$\partial p/\partial n = 0$
B	$\partial B/\partial n = 0$	$\partial B/\partial n = 0$	Fixed value
ϕ	$\phi = 0$	$\partial \phi/\partial n = 0$	$\partial \phi/\partial n = 0$
Re	1000		
Ha	0, 50,100, and 200		

5. RESULTS AND DISCUSSION

Several published study in the available reference are used to verify the accuracy of the present solver. However, the result from the reference (Shercliff, 1953) for the flow through the pipe with the transverse magnetic field is considered as a validation test case. The boundary conditions and wall treatment for the same are taken from the given reference (Shercliff, 1953). The numerical simulation for validation is performed at *Re* = 100, and *Ha* = 0 and 10. The results are compared for the streamwise velocity in the vertical coordinate. Fig. 2(c) shows the comparison of the velocity obtained in the present case with the reference (Shercliff 1953) and shows good agreement. Now we will talk about numerical simulations of MHD flow-through channel with two different orifices (rectangular plate orifice (*Orifice 1*) and triangularly shaped orifice (*Orifice 2*)) for the fixed blockage ratio of β = 1:4. The computation results in terms of streamlines, Lorentz force, velocity variation, pressure drop, skin friction coefficients and dimensionless wall pressure are compared for both orifices under the MHD flow condition. The results are structured in such a way to show the influence of Lorentz force on the flow field characteristics. All simulations are performed at a fixed *Re* of 1000 and flow is remain laminar throughout the computational domain.

Figure 3 illustrates the velocity streamline for both the orifice for various *Ha* numbers. The presence of the orifice plate in the channel greatly affect the flow physics at upstream and downstream of the plate for non-MHD cases (Figs. 3a and 3b). Orifice

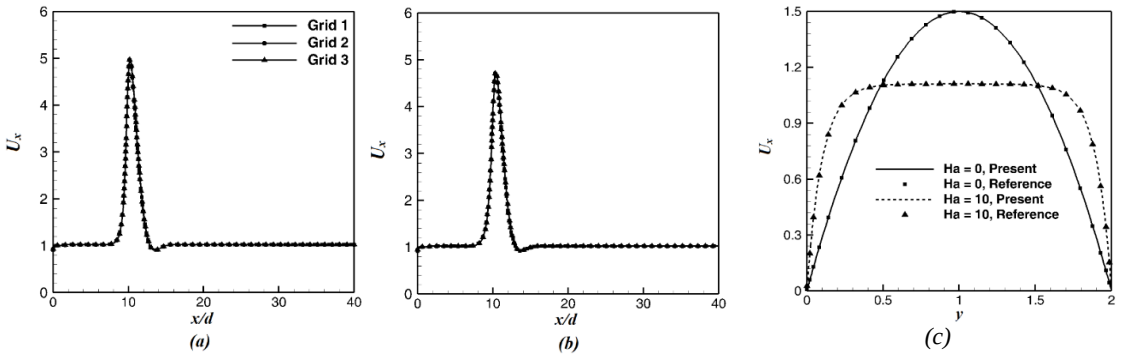

Fig. 2. Comparison of streamwise velocity along the centerline of the channel at *Re* = 1000 and *Ha* = 100 for various grids. (a) Orifice - 1 and (b) orifice - 2. (c) Comparison of streamwise velocity profile in fully developed region for present results with the data available in the reference (Shercliff, 1953).

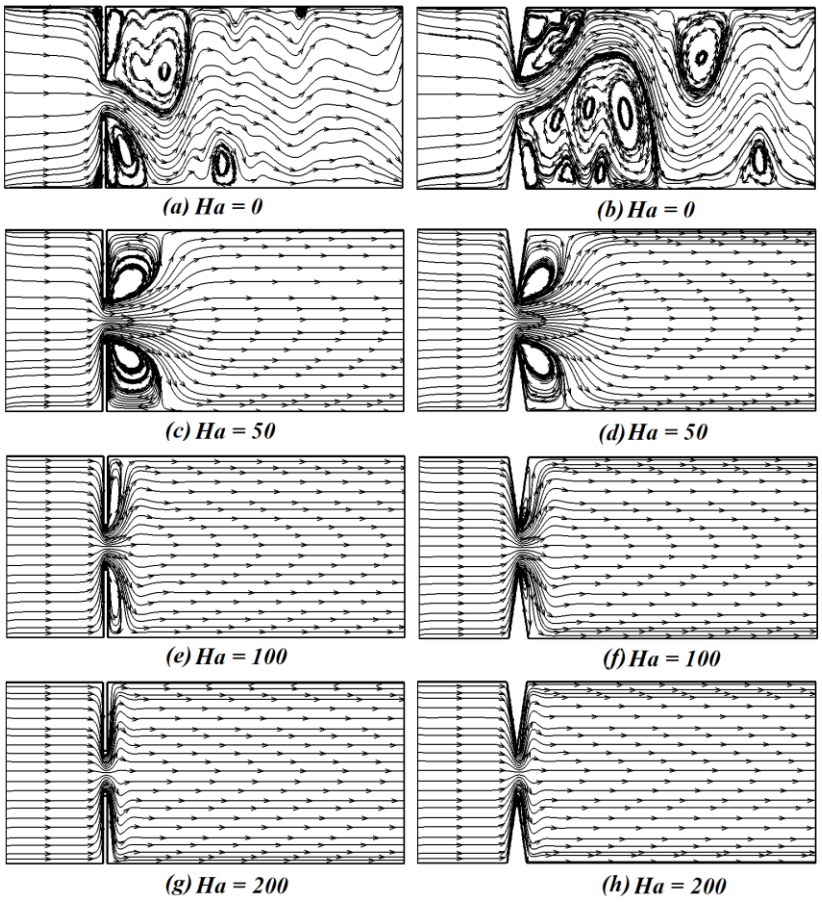

Fig. 3. Streamlines distribution for various *Ha* and at the fixed *Re* of 1000, for (Left) orifice -1, and (Right) orifice - 2.

- 1 and 2 shows significant variation in development of primary and secondary vortices for non-MHD cases and asymmetric flow pattern is observed at *Ha* = 0 for both the orifices. Orifice -1 and orifice 2 shows development of smaller third vortices on the same side of smaller zone of primary eddies. At the throat, both orifice shows high speed jet formation due to the contraction and further downstream flow separation in terms of vortices are observed. Further away from the throat, flow loses speed and carry on till it reaches to fully developed region. In the downstream region, one big size primary eddy is formed along with smaller secondary eddies in both top and bottom side of the channel. The direction of rotation of primary and secondary vortices are reverse to each other. The major drawbacks in the flow through orifice is flow assisted corrosion (FAC) and mechanical wearing of pipeline, is occurred due to cavitation or formation of eddies in the flow near the downstream walls of channel. Many active and/or passive methods are used to control eddies and finally cavitation (Deylami *et. al.*, 2017). It is observed that, in the presence of external magnetic

field, eddies formation, its size and location are significantly control. In the present numerical study application of external magnetic field in the *y*-direction is used as an active control mechanism to suppress the eddy formation in the channel with orifice plates. At a very small *Ha* of 50 the presence of secondary eddies is vanished as observed in Figs. 3c and 3d. The length of primary eddies are also concentrated. Further increased in *Ha* to 100 shows drastic reduction in the length of primary vortices and for *Ha* of 200 (Figs. 3e and 3f)) eddies in the flow is almost vanished. The point of reattachment of flow in the downstream of the orifice shrinks with increases of *Ha* number. The flow becomes fully attached to the top and bottom wall at very short length after the throat area. The observed flow behavior is due to the presence of magnetic field. Electrically conducting fluid produces the electric current when it flows in the magnetic field zone. The fluid flow behavior and the vortices suppression are severely affected by the development of Lorentz force.

The interaction between electric current and magnetic field produce the Lorentz force. The electric potential is developed according to the Ohm's law (Eq. (3)), and the gradient of induced electric potential is proportional to the velocity of the fluid and imposed magnetic field ($\partial\phi/\partial z \simeq UB$). The velocity gradient and magnetic field are developed in the *x* and *y*-direction. Hence the electric potential is produced in the *z*-direction. Similarly, the induced electric current is also flowing in z-direction only. The present case is of two-dimensional with single cell thick in the *z*-direction, hence the electric potential distribution and current flow in the channel are not shown in this study. However, the influence of the electric potential and electric current has its impact on the fluid flow structures by generating the Lorentz force. The generation of Lorentz force ($F_L = \vec{j} \times \vec{B}$) depends on the electric current density ($\vec{j} \approx \vec{U} \times \vec{B}$) and the applied magnetic field ($\vec{B}$). In the present study, the magnetic field is imposed in the *y*-direction (B_y) and the velocity gradient is available in the *x* and *y*-direction (U_x and U_y). The vertical component of velocity (U_y) does not play the significant role in the generation of electric potential (due to less magnitude) and subsequently the electric current ($\vec{j}_z \approx \vec{U}_y \times \vec{B}_y \approx 0$). The interaction between streamwise velocity components (U_x) and the magnetic field in the *y*-direction (B_y) produces the electric potential gradient and hence electric current in the *z*-direction ($\vec{j}_z \approx \vec{U}_x \times \vec{B}_y$). Therefore, the induced Lorentz force is developed in the *x*-direction ($F_{Lx} = \vec{j}_z \times \vec{B}_y \approx -U_x B_y^2$). Here the negative sign implies that the direction of flow of Lorentz force is in the reverse direction to the fluid flow.

Figure 4 illustrates the contour plots of Lorentz force in the computational domain for the various applied magnetic field. The pressure is the driving force for the flowing fluid, and the negative values in the contour plot of Lorentz force indicate the opposing force to fluid pressure. In the MHD flow, the area of higher velocity shows the higher magnitude of Lorentz force (Fig. 4). However, for the same inertia force condition or at same *Re*, the increase in *Ha* number intensified the magnitude of Lorentz force. The maximum value of opposing Lorentz force at *Ha* = 50 is -7 for both the orifice (orifice 1 and 2) as shown in Figs. 4a and 4b). For the highest applied magnetic field (*Ha* = 200), the maximum Lorentz force is -130 and -105 for orifice 1 and 2 respectably as given in Figs. 4*e* and 4*f*. The strength of Lorentz force is higher in the case of orifice 1 than orifice 2 due to the formation of the high-speed jet at the throat. The Lorentz force suppressed the formation of primary and secondary eddies. This shows that the flow separation point shifted gradually towards the orifice throat and vanished at the higher *Ha* number as reported in Figs. 3g and 3h.

Figure 5 shows the directions of developed Lorentz force for the variously applied intensity of magnetic field. It gives the clear effect of suppression of the flow, with the increase in the *Ha* number. The partition line downstream of the orifice in Fig. 5 shows the two different directions of application of Lorentz force concerning the fluid flow. The Lorentz force lines inside the partition line and near to the top and bottom wall has the direction of flow as same as streamlines. The lines in between the two partition or in the core region of the channel have the reverse direction as compared to the fluid flow. The Lorentz force lines which are in the same direction of streamlines show the area of flow reversal. The shrinkage of this area is observed with increasing *Ha* number. To achieve the flow with the uniform layer or flow without any eddy, the magnetic field is adjusted according to the Reynolds number.

Figure 6 reveals the variation of the strength of Lorentz force along the centerline of the channel. The steep change in the Lorentz force at the orifice throat area is due to the high jet velocity at that location and subsequently development of strong Lorentz force. As the *Ha* increased the opposing Lorentz force increases and it is shown in Fig. 6 as the negative peak value observed at *x/d* =10.

Figure 7 illustrates the comparison of the velocity profile for both the orifice at various downstream location (*x/d* = 10, 15, 20, 25 and 30) for the various applied magnetic field. As the flow at *Ha* = 0 is asymmetric, hence velocity comparison for the orifices at *Ha* = 0 is not shown in the present case. The velocity profile obtained for MHD cases has symmetric nature, therefore its comparative analysis is shown in this case. At the throat, high-velocity jet is formed, and the peak of the velocity reaches 6.95 (m/s) and 5.99 (m/s) for orifice1 and 2 respectively for the non-MHD case. After that, the flow pattern at *Ha* = 50 in the downstream flow for both the orifices beyond *x/d* = 10, shows similar velocity distribution. It suggests that beyond this location, flow losses the geometrical influence. After that, the

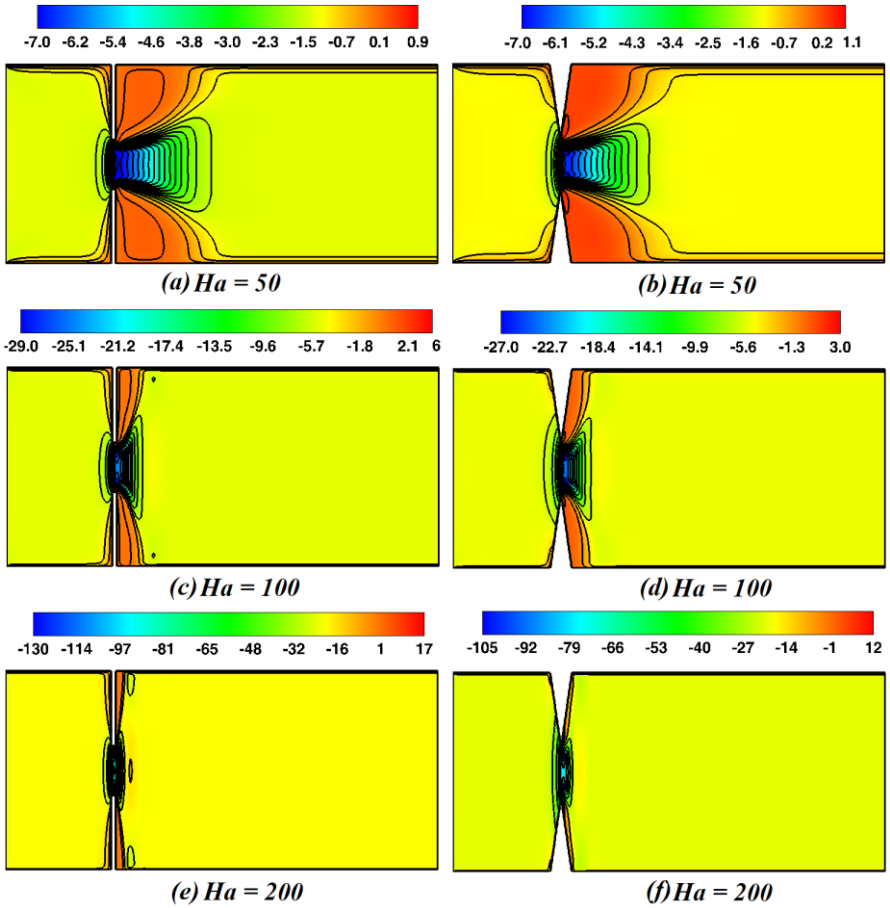

Fig. 4. Lorentz force contours for various *Ha* and at the fixed *Re* of 1000, for (Left) orifice -1, and (Right) orifice-2.

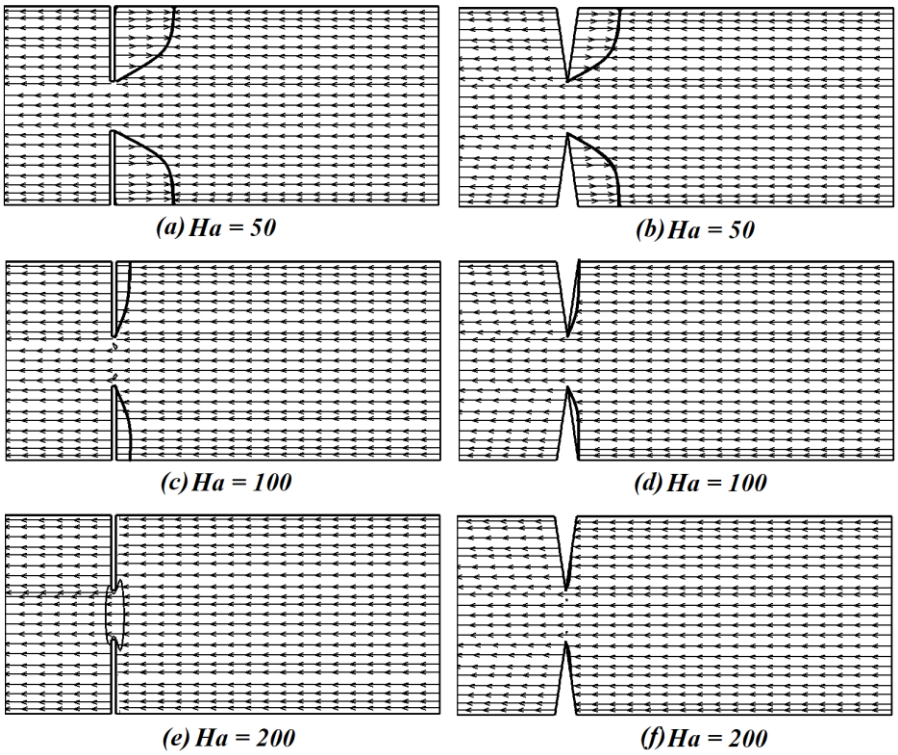

Fig. 5. Lorentz force direction for various *Ha* and at the fixed *Re* of 1000, for (Left) orifice -1, and (Right) orifice-2.

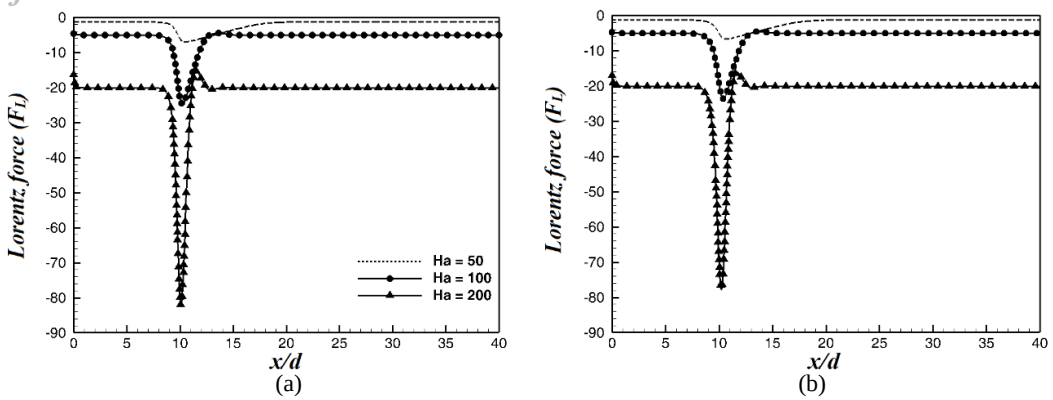

Fig. 6. Lorentz force strength at fixed *Re* = 1000 and various *Ha* at the centerline of the channel, for (a) orifice -1, and (b) orifice - 2.

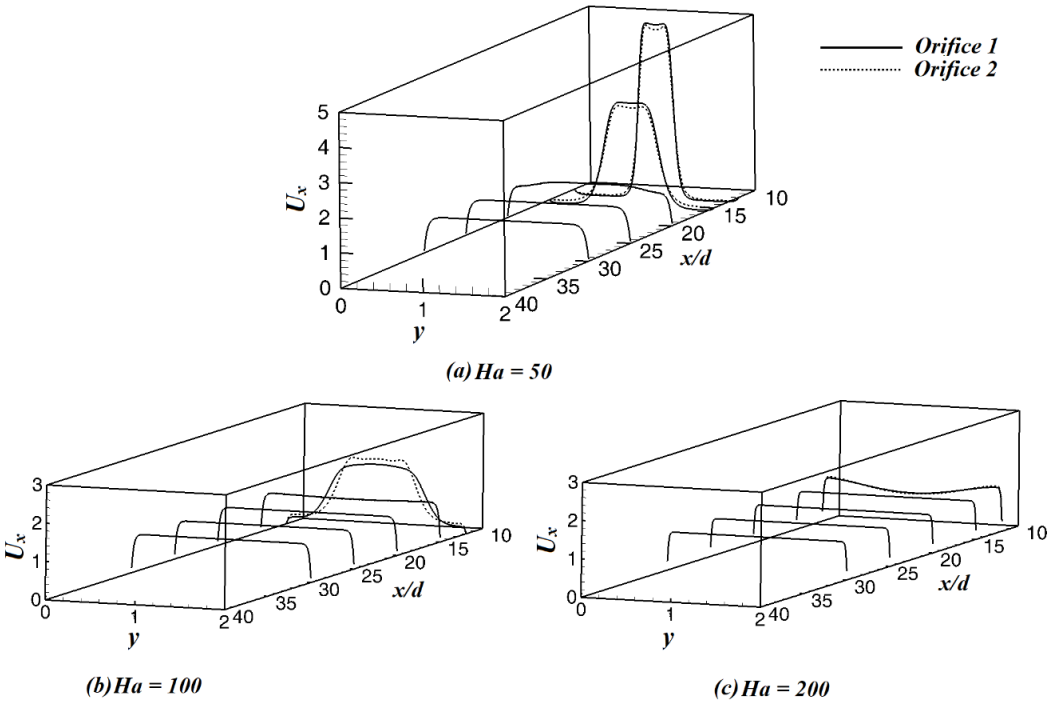

Fig. 7. Comparison of the velocity profile for both the orifices at fixed *Re* = 1000 and various *Ha* at different locations downstream of the orifice.

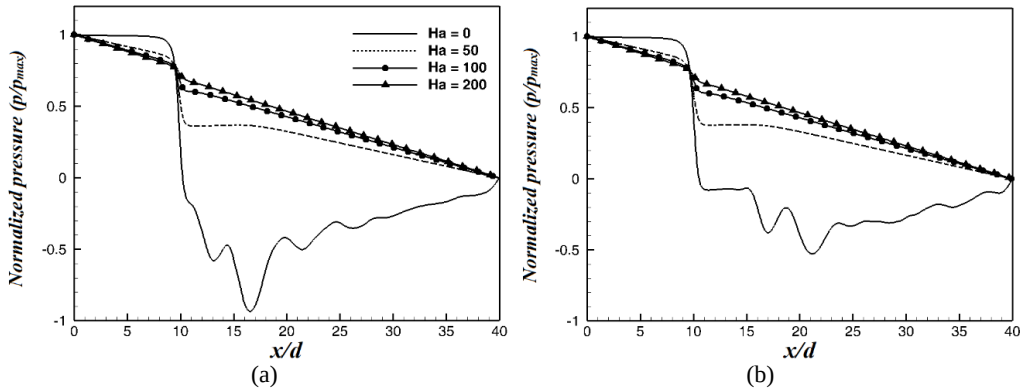

Fig. 8. Normalized pressure variation at a fixed *Re* = 1000 and various *Ha*, (a) orifice 1, and (b) orifice 2.

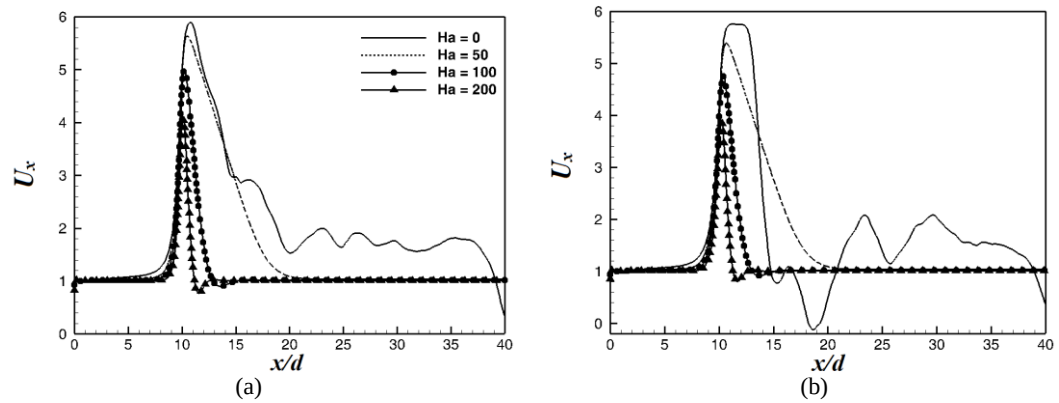

Fig. 9. Axial variation of streamwise velocity at fixed *Re* = 1000 and various *Ha*, (a) orifice 1, and (b) orifice 2.

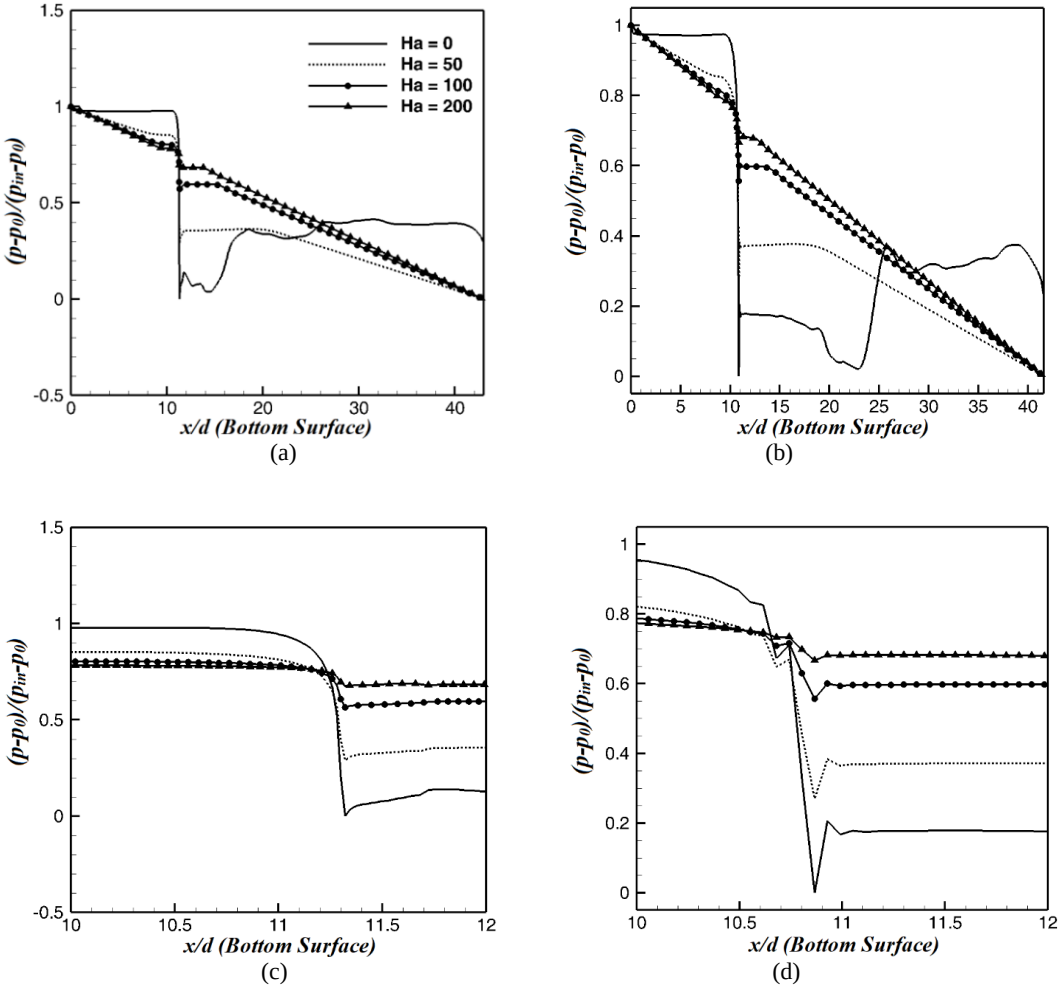

Fig. 10. Dimensionless wall pressure variation along the length on the bottom wall of the channel for various *Ha* (a) orifice-1, (b) orifice-2, (c) and (d) shows close-up view for orifice 1 and 2 respectively.

increased in *Ha* to100, for both orifices, the velocity profile overlaps each other beyond *x/d* = 15. Further increased in *Ha* to 200, even close to the throat at *x/d* = 10 also shows overlap in velocity profile. This trend suggests, at the higher applied magnetic field, the flow become independence of the geometry and show similar velocity distribution.

Figure 8 shows the normalized pressure variation along the centerline of the channel. The normalized pressure variation shows the sharp pressure gradient in the downstream of the orifice plates for non-MHD cases. This reverse pressure gradient is responsible for the cavitation in the channel. The sudden change in the pressure in the downstream of the orifice is reduced as the intensity of the magnetic field rises. For the higher value of *Ha* number (200) the smooth pressure distribution is observed and shows the control of eddy formation and subsequently cavitation. Figure 9 shows the

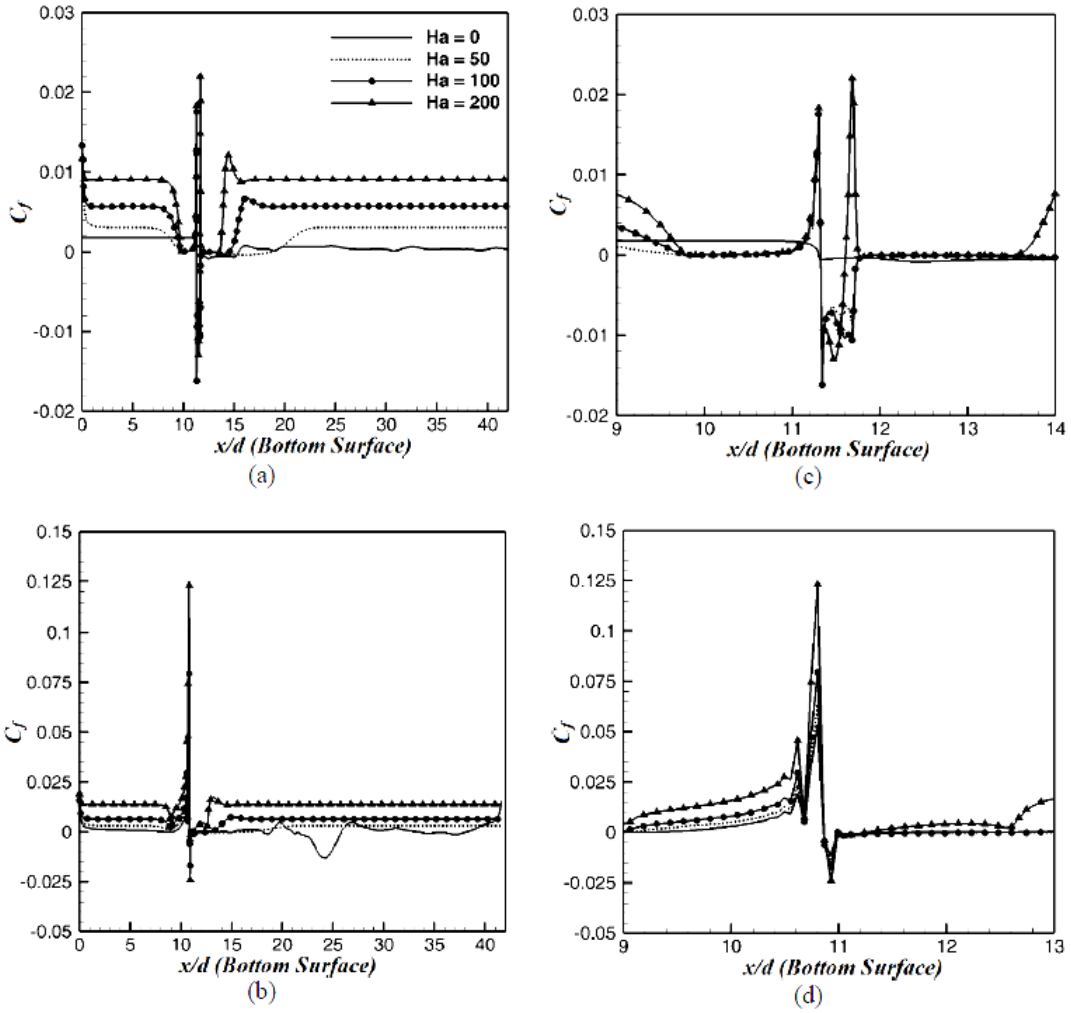

Fig. 11. Skin friction coefficient variation along the arc length on the bottom wall of the channel for various *Ha* (a) orifice-1, (b) orifice-2, (c), and (d) shows close-up view for orifice 1 and 2 respectively.

axial variation of streamwise velocity. The velocity at *Ha* = 0 shows the non-uniform distribution of flow throughout the channel length. The cavitation or erosion and flow assisted corrosion in the channel are the more substantial concern for the flow through orifices for non-MHD flow. The non-uniformity in the flow is controlled by the magnetic field with the increase in the intensity (*Ha* = 50 - 200). The velocity profile for higher *Ha* (50 - 200) shows the uniform pattern along the length of the channel and become fully developed just after the throat at the higher magnetic field (*Ha* = 200).

Figure 10 shows the non-dimensional wall pressure variation over the bottom wall of both orifices for various Ha number. It is observed that the flow separation zone is higher for a non-MHD flow (*Ha* = 0) due to the adverse pressure gradient (negative slope). When the magnetic field is imposed on the system, the slope of the dimensionless wall pressure line shifted towards the favorable (positive) nature at *Ha* = 200. Figure 11 shows the skin friction coefficient (C_f) variation over the bottom wall of the channel for both orifices for various Ha number. C_f shows the drag of the fluid on the surface of the channel and also, it indicates the reattachment point downstream of flow as the drag coefficient shows the positive trends beyond the reattachment point. The reattachment length of flow is higher for the flow at *Ha* = 0 and gets shorter as magnetic field intensity gets increased (*Ha* = 200). The C_f is highly affected by the magnetic field near the throat area as well as on the entire surface of the channel as shown in the close-up view (Figs. 11 c and 11d). This is so because the fluid is forced to flow near the wall as the magnetic field is applied to the system. It is due to the induce Lorentz force in this zone and is highly opposing in nature to the flow of fluid, and fluid tends to flow near the wall.

Table 2 shows the reattachment length of the flow downstream of the orifice. It is found that the reattachment length in the downstream of the orifice reduces as the intensity of magnetic field raised. The reattachment length is reduced approximately by 93% and 95% for *Ha* of 200 with respect to *Ha* = 0 for orifice 1 and orifice 2 case respectively. Flow reattached with the surface just after leaving the orifice in the case of flow through channel with orifice 2 at *Ha* = 200.

Table 2 Reattachment length for both orifice cases

Hartmann number (*Ha*)	Reattachment length downstream of orifice	
	Orifice-1	Orifice-2
Ha = 0	8.7*d*	7.10*d*
Ha = 50	5.7*d*	4.8*d*
Ha = 100	1.5*d*	1.2*d*
Ha = 200	0.6*d*	0.3*d*

5. CONCLUSION

The flow field behavior in the presence of external magnetic field have been numerically investigated for the flow through channel with two type of orifices (rectangular plate and triangular shaped orifice). The results are obtained for various *Ha* number (0, 50, 100 and 200) and for the fixed Reynolds number of 1000. Due to the application of external magnetic field, the formation of primary and secondary eddies are suppressed. As the intensity of magnetic field in terms of *Ha* number increased to 200, entire computational domain shows smooth flow of fluid without any trace of vortices. The developed Lorentz force opposes the fluid flow and control the flow separation. Hence, the asymmetric nature or chaos in the fluid is suppressed and fluids are allowed to flow in smooth pattern in the downstream of orifice without any vortices. As the flow is in uniform layers, the problem associated with channel like, erosion, cavitation, and flow assisted corrosion is under control, and lifespan of the channel can be further improved. It is observed that due to the imposed magnetic field, at higher Ha number, flow losses the geometrical effect and show similar behavior after x/d = 10 for both considered orifice plates. One can use MHD as an active flow control alternate to another type of passive and active method without modifying or redesigning the geometry.

ACKNOWLEDGMENT

Authors are thankful to Government of India for providing the research set up and financial aid to conduct the present study.

REFERENCES

Abdulrazaq, A. A. Hasan, M. B. and H. A. Wael (2017). Investigation of flow through multi-stage restricting orifices, *Ann. Nucl. Energy* 104, 75-90.

Altintas, A. and I. Ozkol (2015). Magnetohydrodynamic Flow of Liquid-Metal in Circular Pipes for Externally Heated and Non-Heated Cases, *Journal of Applied Fluid Mechanic* 8(3), 507-514.

Aleksandrova, S. and S. Molokov (2012). The structure of parallel layers in steady two-dimensional magnetohydrodynamic flows in sudden duct expansions and contractions. *Theor. Comput. Fluid Dyn*. 26, 29-35.

Ahmed, W. H. (2010). Evaluation of the proximity effect on flow-accelerated corrosion. *Ann. Nucl. Energy* 37, 598–605.

Deylami, H. M. Amanifard, N. Hosseininezhad, S. S. and F. Dolati (2017). Numerical investigation of the wake flow control past a circular cylinder with Electrohydrodynamic actuator. *Eur. J. Mech. B/Fluids* 66, 71-80.

El Khoury, G. K., M. Barri, H. I. Anderson and B. Pettersen (2010). DNS of Orifice Flow with Turbulent Inflow Conditions. *Proceeding of Direct and large-Eddy simulation VII*, 13, 81-84.

Feng, J., Q.He, H. Chen, M. Ye (2016). Numerical Investigation of magnetohydrodynamic flow through sudden expansion pipes in Liquid Metal Blankets. *Fusion. Eng. Des* 109-111, 1360-1364.

Fujisawa, N., N. Kanatani, T. Yamagata and T. Takano (2015). Mechanism of non-axisymmetric pipe-wall thinning in pipe line with elbow and orifice under influence of swirling flow. *Nucl. Eng. Des* 285, 126–133 (a).

Fujisawa, N., T. Yamagata, N. Kanatani and R. Watanabe (2015). Non-axisymmetric wall-thinning downstream of elbow-orifice in swirling flow. *Ann. Nucl. Enegy* 80, 356–364 (b).

Ferziger, J. H. and M. Peric (2002). *Computational Methods for Fluid Dynamics*. Third edition, Springer.

Haimin, W., X. Shujuan, S. Qingyi, Z. Caimin, L. Hao and C. Eryun (2013). Experimental study on pressure drop of a multistage letdown orifice tube. *Nucl. Eng. Des* 265, 633-638.

Hollingshead, C. L., M. C. Johnson, S. L. Barfuss and R. E. Spall (2011). Discharge coefficient performance of Venturi, standard concentric orifice plate, V-cone and wedge flow meters at low Reynolds numbers. *J. Pet. Sci. Eng* 78(3–4), 559–566.

Hwang, K. M., T. E. Jin and K. H. Kim (2009). Identification of relationship between local velocity components and local wall thinning inside carbon steel piping. *J. Nucl. Sci. Technol* 46, 469–478.

Kain, V. (2014). Flow Accelerated Corrosion: Forms, Mechanisms and Case Studies. 1st

International Conference on Structural Integrity, *Procedia Engineering* 86, 576 – 588.

Mardkari, F., M. Aghakhani and E. Esmaeilzadeh (2012). Experimental study of fluid flow around cylinder in the presence of EHD actuators. *J. Appl. Sci* 12, 90–95.

Mistrangelo, C. and L. Buhler (2007). Numerical investigation of liquid metal flows in rectangular sudden expansions. *Fusion. Eng. Des* 82, 2176-2182.

Morrison, G. L., R. E. DeOtte, G. H. Nail and D. L. Panak (1993). Mean velocity and turbulence fields inside a β=0.5 orifice flowmeter. *AIChe J* 39(5), 745-756.

Praveen, T. and V. Eswaran (2017). Transition to asymmetric flow in a symmetric sudden expansion: Hydrodynamics and MHD cases. *Comput Fluids* 148, 103-120.

Shan, F., L. Zhichun, L. Wei and T. Yoshiyuki (2016). Effects of the orifice to pipe diameter ratio on orifice flows. *Chem Eng Sci* 152, 497–506.

Singh, V. K. and T. John Tharakan (2015). Numerical simulations for multi-hole orifice flow meter. *Flow Meas. Instrum* 45, 375–383.

Shah, M. S., J. B. Joshi, A. S. Kalsi, C. S. R. Prasad and D. S. Shukla (2012). Analysis of flow through an orifice meter: CFD simulation. *Chem. Eng. Sci* 71, 300–309.

Smolentsev, S. (2009). MHD duct flow under hydrodynamic "slip" condition. *Theor. Comput. Fluid Dyn* 23, 557–570.

Sreenivasan, B. and T. Alboussiere (2000). Evolution of a vortex in a magnetic field, *Eur. J. Mech. B - Fluids* 19, 403–421.

Sydberger, T. and U. Lotz (1982). Relation between mass transfer and corrosion in a turbulent pipe flow. *J. Electrochem. Soc* 129, 276–283.

Shercliff, J. A. (1953). Steady motion of conducting fluids in pipes under transverse magnetic fields. Mathematical *Proceedings of the Cambridge Philosophical Society* 49, 136-144.

Utanohara, Y., Y. Nagaya, A. Nakamura and M. Murase (2012). Influence of local flow field on flow accelerated corrosion downstream from an orifice. *J. Power Energy Syst* 6, 18–33.

Vantieghem, S., X. Albets-Chico and B. Knaepen (2009). The velocity profile of laminar MHD flows in circular conducting pipes. *Theor. Comput. Fluid Dyn* 23, 525–533.

Yakeno, A., S. Kawai, T. Nonomura and K. Fujii (2015). Separation control based on turbulence transition around a two-dimensional hump at different Reynolds numbers, *Int. J. Heat Fluid Flow* 55, 52–64.